BUILD SIMUL (2015) 8: 381 – 392
DOI 10.1007/s12273-015-0219-6

Air and air contaminant flows in office cubicles with and without personal ventilation: A CFD modeling and simulation study

Meng Kong (✉), Jianshun Zhang, Jingjing Wang

Department of Mechanical Engineering, Syracuse University, 263 Link Hall, Syracuse, NY 13244, USA

Abstract

The paper is aimed at building an appropriate computational fluid dynamics (CFD) model for simulating the flow field in the office cubicle with and without personalized ventilation (PV) and using it to investigate the flow field in the cubicle. A computational model was first constructed by using a commercial CFD code (STAR-CCM). In this process, different approaches to represent manikins, boundary conditions, geometries, and gridding were tested, and a proper approach was selected for simulating the air and contaminant movement in the cubicles and their interactions with the remaining room space. A comparison between the simulation and the experimental results are made to show how accurate the CFD model can be. A brief evaluation of the environmental quality was conducted for both cases with PV and underfloor air diffuser (UFAD). This comparison showed a significant advantage in the PV system, indicating how the PV system performed under different airflow rates. This verified CFD model will be utilized in the future to investigate the performance of the partitioned cubicle collaborating with personalized ventilation systems.

Keywords

personalized ventilation,
CFD,
thermal plume,
cubicle

Article History

Received: 28 October 2014
Revised: 23 February 2015
Accepted: 26 February 2015

1 Introduction

1.1 Background

Thermal comfort and air quality are two important aspects of indoor environmental quality (IEQ). The heating, ventilating, and air-conditioning (HVAC) system determines energy and air exchange in buildings. Building occupants also participate in setting the room's environmental conditions by exchanging energy with the building. By the thermoregulatory process, the body core temperature is kept around 37℃ (98.6°F) (Vander et al. 1994), and the surface temperature varies between 29℃ and 35℃ (Dygert and Russo 2009; Houdas and Ring 1982). Since a temperature difference exists between the body surface and the ambient air, the buoyancy results in a thermal boundary around the human body moving upward. This thermal boundary layer around human body and the resulting thermal plume above it play a key role in the determination of the heat flux and the contaminant concentration distribution in the vicinity of the body.

In most buildings, clean and cool air is often supplied to an occupied space by both mixing and displacement ventilation systems. Often, occupants in rooms with mixing or displacement ventilation have to compromise between preferred thermal comfort and perceived air quality because some people are very sensitive to air movement while others are sensitive to the air quality. The disadvantage of the total-volume ventilation principle is that often room air movement is changed due to furniture rearrangement, which may increase occupants' complaints of draught and/or poor air quality (Melikov et al. 2002). In contrast to total volume ventilation, personalized ventilation (PV) aims at supplying clean and cool outdoor air directly to the occupants. Kaczmarczyk et al. (2004) indicate that PV is capable of improving the thermal comfort and air quality around the subject, reducing the intensity of SBS symptoms and thereby increasing subjects' productivity. Since personalized ventilation can satisfy the individual needs of each occupant by customizing the environment around the body, it has a big advantage over both displacement and mixing ventilations. It was also found that a PV system supplying an amount of fresh air four times smaller than the displacement ventilation could be more effective in terms of users' satisfaction (Cermak et al. 2011; Gao and Niu 2005) and could also reduce cooling

E-mail: mkong01@syr.edu

List of symbols

c_p	specific heat capacity (J/(kg·℃))	T_s	temperature of the supply air (℃)
C	tracer gas concentration at target point (kg/m^3)	T	mean temperature (K)
C_e	tracer gas concentration in the exhaust (kg/m^3)	T_p	temperature at target point (℃)
C_s	tracer gas concentration in the supply air (kg/m^3)	T'	fluctuating temperature (K)
d_k	diffusion of turbulent kinetic energy (W)	u_i	mean velocity along i-th direction (m/s)
G_k	gravity production of turbulent kinetic energy (W)	u_i'	fluctuating velocity along i-th direction (m/s)
h_{teq}	dry heat transfer coefficient (W/℃)	x_i	coordinate in i-th direction (m)
H_i	turbulent heat diffusion term (W/m^2)	y^+	dimensionless wall distance
k	turbulent kinetic energy (J)	γ_t	thermal turbulent diffusivity (m^2/s)
l_μ, l_ε	characteristic lengths (m)	Γ	corresponding diffusion coefficient
p	hydrostatic pressure (Pa)	ε	turbulence dissipation rate (W)
P_k	shear production of the turbulent kinetic energy (W)	μ	dynamic viscosity (Pa·s)
q''_t	measured heat loss (W)	μ_t	turbulent viscosity (Pa·s)
S	corresponding source term	ν_t	eddy viscosity (m^2/s)
S_j	momentum source term (N/m^3)	ρ	density (kg/m^3)
t	time (s)	τ_{ij}	Reynolds' stress (kg/(m·s^2))
t_{eq}	equivalent temperature (℃)	ϕ	time averaged part of scalar variable (energy, enthalpy, concentration, etc.)
t_s	manikin surface temperature (℃)		
T_{clo}	temperature of the clothes surface (℃)	ϕ'	fluctuating part of scalar variable

and heating power consumptions by approximately 75% and 61%, respectively (Chludzinska and Bogdan 2008). The same conclusion was obtained by Melikov et al. (2002) that PV may decrease significantly the number of occupants dissatisfied with inhaled air quality. The ability of PV to deliver clean, cool, and dry air to the breathing zone of each occupant and maintain the thermal comfort level depends on the interaction among the airflow generated by PV, occupant-initiated flows (free convection flow around the body and the flow of respiration), the airflow of exhalation, and the room airflow outside workspaces (Melikov 2004).

Several kinds of personalized ventilation devices have been developed recently. Some of them can improve the air quality as well as thermal comfort while others cannot. For example, a push-and-pull type of PV invented and applied to aircraft cabin seats showed a dramatic decrease (77%) of contaminant concentration inhaled by the exposure manikin when the local supply with clean air existed and the contaminant exhaled can only be exhausted effectively when the local exhaust and the local supply are used simultaneously (Melikov and Dzhartov 2013). A local exhaust ventilation system with a privacy cell in the air cabin developed by Dygert and Dang (2012) also show an advantage compared to backseat exhaust, reducing the passenger exposure to 60% no matter where the infectious source is. Many personalized ventilation terminals have been developed and tested by Nielsen et al., and the performance of these systems proved significant (Nielsen et al. 2007a, b, c; 2008; 2013).

1.2 Purpose

Recently the advantage of personalized ventilation system on fulfilling the indoor environment requirement and reducing energy consumption has been gradually accepted by people in practice. However, different with the layout PV was usually tested in the chamber, PV was popularly mounted in the cubicles with partition between each other. This typical arrangement of the office space not only gives relatively independent environment on the remaining office space and other cubicles but allows the interaction between them. Depending on the configuration of the cubicle, layout of the furniture (Zhuang et al. 2014) and air distribution system, the environment in the cubicle, as well as around the manikin, may differ a lot and influence the thermal sensation and inhaled air quality in the breathing zone. Instead of individually testing the performance of the personalized ventilation system, this study is aimed at investigating the collaboration of the personalized ventilation system with the cubicle configuration in terms of thermal comfort and air quality as well as developing a CFD model with acceptable accuracy and satisfactory prediction for future study.

2 Method and procedure

2.1 Overview

The prototype room studied is an office room (625.0 cm ×

1052.0 cm × 315.0 cm) with 12 cubicles arranged in 2 rows, located in the Syracuse Center of Excellent (COE) Building (Fig. 1). Each cubicle has approximately the same configuration and size (191.0 cm × 184.0 cm × 171.0 cm). The target cubicle also contains a manikin. A grid mesh was created using Pointwise, and grid sensitivity was examined. The air and air contaminant movement in the cubicle was simulated by using STAR-CCM. The CFD model was validated by experimental results as well as verified by sensitivity analysis for model parameters. Analysis of the flow characteristics in the cubicle was conducted to quantify the driving forces and their respective impacts on the performance of the personalized ventilation. Cooling/heating efficiency and air quality index (AQI) (Russo 2010) were calculated to evaluate the environmental quality and ventilation performance.

2.2 Experiment setup

Experiments were conducted to give us some basic ideas of the flow field as well as validate the CFD model. A cubicle (191.0 cm × 184.0 cm × 171.0 cm) on the west side of the office (right in Fig. 1; Cubicle G in Fig. 3) with a 84.0 cm wide opening to the corridor was selected to be the test cubicle. A 20-body-segment thermal manikin was used to simulate a real person. The manikin was seated in an office chair in front of the computer approximately 10.0 cm from the front edge of the desk. A side desk and a storage box were placed at the left side of the chair. A monitor with a keyboard and a mouse was placed on the front desk, and a processor was placed beneath the front desk (Fig. 3). Fresh and clean air was supplied to the work place through UFAD (Fig. 2(a)) or PV (Fig. 2(b)) which yielded airflow rates of 9.4 L/s and 55.1 L/s at temperatures of 15.7℃ and 15.3℃, respectively. The UFAD was mounted on the floor of the cubicle fed by a variable-air volume box in the under-floor plenum. The UFAD diffuser consisted of 16 long slots and 16 short slots arranged in a ring of a 6.4 cm internal diameter and a 19.7 cm external diameter. The PV diffuser was mounted 133.4 cm above the floor with a tube connected from back to the air handler. It had a total length of 36.8 cm and a diameter of 6.9 cm with two grill openings placed symmetrically on both

Fig. 1 Target cubicle (left) and TIEQ (right)

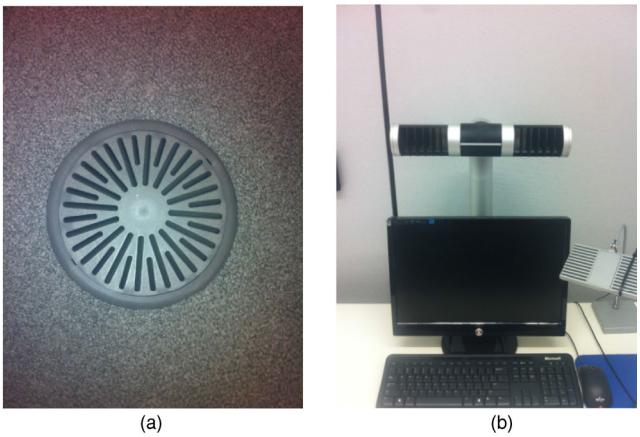

(a) (b)

Fig. 2 Terminal of ventilation system: (a) UFAD, (b) PV

wings. Each opening was 11.4 cm long and had a grill divided into 6 equal parts (Table 1). The supply air direction was adjusted by rotating each wing about the central axle of the diffuser. During the test, a manikin in normal winter clothing (around 0.6 clo) was set a comfort mode, which resulted to the manikin could maintain the skin temperature at the temperature as in comfortable condition by controlling the heat flux. Both the temperature and heat flux of the manikin were monitored and recorded during the experiment.

During the experiment, the flow field around the manikin was monitored in terms of both velocity and temperature at different heights (0.1 m, 0.6 m, 0.8 m, 1.1 m, 1.4 m, and 1.6 m) and locations (left front, left, right front and right) using the spherical anemometer with an accuracy of 0.02 m/s and 0.2℃. The velocity in front of the PV was also measured to validate the CFD model.

2.3 Governing equations for CFD model

The eddy-viscosity RANS model is the most popular class of turbulence model utilized for indoor environment simulations (Dygert and Russo 2009). The basic equations include the transport equation of mass, momentum, and other quantities.

$$\frac{\partial}{\partial x_i}(\rho u_i) = 0 \tag{1}$$

$$\frac{\partial}{\partial t}(\rho u_j) + \frac{\partial}{\partial x_i}(\rho u_i u_j) = -\frac{\partial p}{\partial x_j} + \frac{\partial}{\partial x_i}\left(\mu \frac{\partial u_j}{\partial x_i} - \rho \overline{u'_j u'_i}\right) + S_j \tag{2}$$

$$\frac{\partial}{\partial t}(\rho \phi) + \frac{\partial}{\partial x_i}(\rho u_i \phi) = \frac{\partial}{\partial x_i}\left(\Gamma \frac{\partial f}{\partial x_i} - \rho \overline{u'_i \phi'}\right) + S \tag{3}$$

Boussinesq and Reynolds' analogies are used to model the turbulent term.

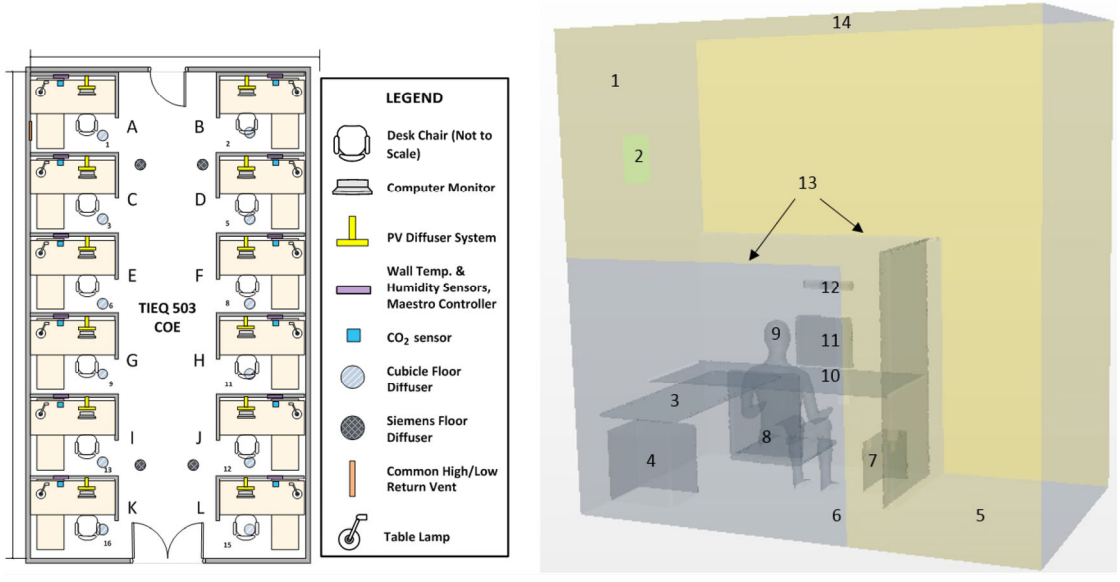

Fig. 3 Cubicles configuration (1. wall; 2. exhaust opening; 3. side desk; 4. storage box; 5. floor; 6. floor diffuser; 7. computer processor; 8. chair; 9. manikin; 10. front desk; 11. monitor; 12. PV diffuser; 13. cubicle partition; 14. ceiling)

Table 1 Configuration parameters of the cubicle

	Dimension (m)	Location (m)
Cubicle	191.0 cm × 184.0 cm × 171.0 cm with a 84.0 cm wide opening to the corridor	West side of the office, Cubicle G
Front desk	74.0 cm × 177.0 cm	8.0 cm away from the front partition
Manikin	135.0 cm high seated manikin	10 cm away from the front desk at chest height
Side desk	152.0 cm × 58.0 cm	13.0 cm away from the west wall
Monitor	44.0 cm × 30.0 cm × 3.0 cm	36.0 cm away from the front partition
PV	Diameter: 6.9 cm, 36.8 cm long with two 11.4 cm long grill openings	1.33 m above the floor and 0.34 m away from the front partition
UFAD	16 × 6.5 cm long slots and 16 × 4.0 cm short slots arranged in a ring of a 6.4 cm internal diameter and 19.7 cm external diameter	Center of the diffuser is 37.0 cm away from the back partition and 20.0 cm from the opening of the cubicle
Storage box	41.0 cm × 18.0 cm × 36.0 cm	18.0 cm away from the front partition and 10 cm from the side partition

$$\tau_{ij} = -\rho\overline{u_i' u_j'} = \mu_t \frac{\partial u_i}{\partial x_j} \tag{4}$$

$$H_i = \rho c_p \overline{u_i' T'} = -\rho c_p \gamma_t \frac{\partial T}{\partial x_i} \tag{5}$$

For RANS-based CFD methods, the most difficult task in setting up a CFD simulation is the selection of the turbulence model. Researchers have used a wide range of turbulence models when studying the microenvironment around the human body (Dygert and Russo 2009) including the zero-equation model (Chen and Xu 1998), standard k-ε model (Gao and Niu 2004; Hayashi et al. 2002), the RNG k–ε model (Gao and Niu 2006; Khalifa et al. 2006), the v^2–f model (Dang 2008), the realizable k–ε model (Russo et al. 2009), and the SST k–ω model (Deevy et al. 2008). By comparing different turbulence models including k–ε family and k–ω family models, Dygert and Russo (2009) found the k–ε family gave similar predictions and compared well with his test data, while k–ω turbulence models did not match with the test data in predicting the jet development. In this case the realizable k–ε turbulence model was used.

Another challenge in modeling room airflows by CFD is the simulation of flow close to solid surfaces since turbulent flow transits to laminar flow when it gets close enough to the surfaces. The two-layer approach, developed by Xu and Chen (2001), is used as an alternative to the low-Reynolds' number approach that allows the one-equation turbulence model to be applied in the near-wall region and the two-equation k–ε model to be applied in the region away from the wall. With this approach, the whole flow field is divided into two regions—the near-wall layer and the

far field. In the near-wall layer, the turbulent kinetic energy k is calculated by

$$\frac{\partial k}{\partial t} + u_i \frac{\partial k}{\partial x_i} = d_k + P_k + G_k - \varepsilon \tag{6}$$

The eddy viscosity is calculated by

$$\nu_t = \sqrt{\overline{u'u'}} l_\mu \tag{7}$$

The turbulence dissipation rate ε by

$$\varepsilon = \frac{\sqrt{\overline{u'u'}} k}{l_\varepsilon} \tag{8}$$

where G_k is the gravity production of turbulent kinetic energy, P_k is the shear production of the turbulent kinetic energy, and l_μ and l_ε are characteristic lengths that are defined in (Xu and Chen 2000).

The values of ε specified in the near-wall layer are blended smoothly with the values computed from solving the k–ε equations far from the wall. The equation for turbulent kinetic energy is solved in the entire flow. This explicit specification of ε and μ_t is arguably no less empirical than the low-Reynolds' number approach, and the results are often as good or better. In STAR-CCM, the two-layer formulations will work with either low-Reynolds' number type meshes $y^+ \sim 1$ or wall-function type meshes $y^+ > 30$ (STAR-CCM 2012).

2.4 Post processing

Air quality index (AQI) (Russo 2010) was used in this paper to indicate the level of air quality. It is defined as

$$\mathrm{AQI} = \frac{1 - C - (1 - C_e)}{1 - C_s - (1 - C_e)} = \frac{C_e - C}{C_e - C_s} \tag{9}$$

AQI is hence a measure of how effectively the fresh supply air is delivered to the target point (e.g., the breathing zone).

In this work, SF_6 was used as the tracer gas emitted from the floor. Because the supply air of the PV system is 100% outdoor air, when AQI = 1.0, clean air is present at the target point, and when AQI = 0.0, the air is perfectly mixed (as it would be in an ideal mixing-ventilation system). The smaller AQI means worse air quality. AQI is converted to ventilation efficiency (VE) or contaminant removal efficiency (CRE) by

$$\mathrm{VE} = \mathrm{CRE} = \frac{C_e - C_s}{C - C_s} = \frac{1}{1 - \mathrm{AQI}} \tag{10}$$

Cooling efficiency of the ventilation system was examined using Cooling/Heating Efficiency Index Φ, a measure of the extent to which the cool supply air reaches the target point (e.g., occupied zone),

$$\Phi = \frac{T_p - T_{clo}}{T_s - T_{clo}} \tag{11}$$

3 Results and discussion

3.1 Verification and validation

A computational model was developed using a commercial CFD code (STAR-CCM). To simulate the flow field in the cubicle, a seated computer simulated manikin (SCSM) was imported into STAR-CCM. In order to model the local airflow in the personal microenvironment of the human body, the configuration of the SCSM was developed by Khalifa et al. (2009), and represented the real shape of the manikin used in the experiment (Villi and Carli 2014). A single cubicle case was created to represent the target cubicle. Polyhedral mesh was used in this study instead of the tetrahedral mesh because it can provide a balanced solution for complex mesh generation problems, and it is relatively easy and efficient to build, requiring no more surface preparation than the equivalent tetrahedral mesh and containing approximately four times fewer cells than a tetrahedral mesh for a given starting surface (STAR-CCM 2012).

To obtain valid simulation results, an appropriate grid is necessary. Increasing the number of cells results in better accuracy as well as much more time for computing. Therefore an optimal mesh is necessary to balance time consumed and the accuracy of the calculation. Creating a grid mesh requires meshing the surface of the manikin first. Then a proper boundary layer representation can be employed on the manikin surfaces. Afterwards the remaining surfaces including walls, inlets, outlets and floor need to be meshed and the volume mesh will be created. Five grids were created for the grid independence study. A summary of the five grids is provided in Table 2. All the cases consist of polyhedral cells with polygonal surface elements, with prism layers attached on the boundary (Fig. 4).

The accuracy of the calculation mostly depends on the density of volume mesh grids. In STAR-CCM, the volume of the mesh grid is controlled by the base size with an allowable ratio range compared to the base size. The velocities in front of the manikin's face were compared (Fig. 4). Cases with base grid size 0.05 m, 0.02 m and 0.015 m gave acceptable grid independence, and were better than 0.07 m and 0.1 m. Considering the time consumed in the simulation, a base grid size of 0.05 m was used.

Always in a ventilation CFD model, the boundary condition at the diffuser outlet also affects the accuracy of the simulation. In order to represent the supply condition more accurately, velocity profile was measured throughout both

Table 2 Grid summary

Grid label	Base size (m)	Number of cells	Number of elements on the manikin	Prism layer	Average wall y^+
A	0.1(**0.1**)	107 846	2 128	5	1.21
B	0.07(**0.07**)	181 925	3 966	5	1.18
C	0.05(**0.05**)	336 326	4 290	5	1.58
D	0.05(**0.02**)	929 342	4 617	15	1.51
E	0.05(**0.015**)	1 857 385	7 556	15	1.42

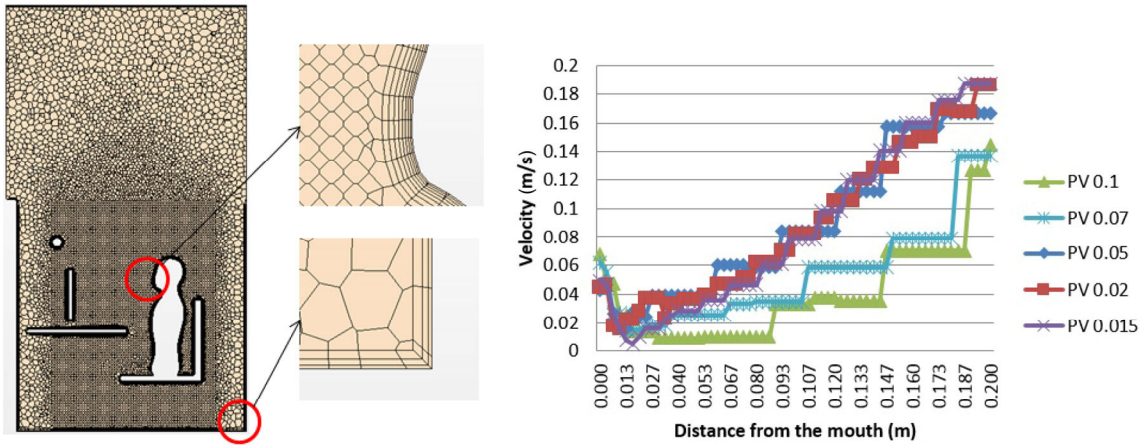

Fig. 4 (a) Grid resolution and (b) velocity in front of the face

the PV and UFAD diffuser openings (Fig. 9). The UFAD velocity profile was measured by slot. Five measuring points were set along each long slot and three measuring points were set along each short slot. Each of the PV openings is divided into 6 parts and 10 (2×5) points' velocity measurement were taken for each part.

In order to validate the simulation model, several cases were conducted and used to compare with the experimental results. Since in the experiment, a thermal comfort mode as well as casual winter clothing were applied to the manikin, a completely identical boundary condition could not be created in the CFD model. Instead, two approximation methods were used to replace the thermal comfort boundary condition: specified heat flux and specified surface temperature by body segment with the same measured surface temperature of other objects (Table 3). To save the simulation time, a single cubicle case was created to compare with a whole room case consisting of totally 12 cubicles with different supply conditions (Table 4). In the single cubicle case, it was assumed that the condition of each cubicle was identical and, the interface conditions between the target cubicle and the two adjacent cubicles were repeated. Although in practice, this assumption is not always true, the result still showed an acceptable agreement with the experimental result which might be because the flow field outside the cubicle did not affect the flow field in it so much.

Table 3 Manikin boundary condition

Parts	PV		UFAD	
	Temp (℃)	Q/A (W/m^2)	Temp (℃)	Q/A (W/m^2)
Face	30.0	126.6	32.5	81.2
Head	31.8	95.5	32.5	82.8
R upper arm	31.4	51.8	32.6	64.0
L upper arm	31.4	55.8	32.6	54.9
R forearm	34.0	50.6	33.6	53.8
L forearm	33.7	67.0	34.5	67.9
R hand	32.5	81.2	32.4	84.0
L hand	32.5	84.6	32.4	84.3
Chest	31.4	72.5	32.3	60.1
Shoulders	34.4	47.7	34.2	51.4
Stomach	34.6	44.1	34.2	50.5
Back	33.0	50.4	31.1	64.9
R up thigh	32.0	34.5	30.2	41.3
L up thigh	32.0	34.9	30.2	37.1
R low thigh	32.9	40.3	30.6	45.6
L low thigh	33.6	39.5	31.6	43.9
R calf	29.3	49.8	30.0	49.1
L calf	29.5	48.0	30.2	47.3
R foot	29.0	47.2	34.5	45.4
L foot	29.2	51.4	31.2	49.6
Wall	24.0		23.9	
Ceiling	26.1		25.5	
Computer processor	25.9	N/A	25.6	N/A
Floor	22.6		23.2	
Monitor	25.7		25.0	
Supply air temp	18.4		18.6	

Table 4 Cubicle setting for whole room simulation

UFAD @ 75℉ (a person seated in the cubicle D)						
	A	B	C	D	E	F
Flow rate (L/s)	55.8	58.8	46.5	48.8	18.2	42.2
SA* Temp (℃)	25.1	25.0	29.0	24.3	23.7	24.4
RA Temp (℃)			24.2			
	G (manikin)	H	I	J	K	L
Flow rate (L/s)	55.1	46.4	42.5	43.7	44.2	55.8
SA Temp (℃)	15.3	24.4	24.6	15.9	24.5	24.7
RA Temp (℃)			24.2			
PV @ 75℉ (a person seated in the cubicle D)						
	A	B	C	D	E	F
Flow rate (L/s)	7.4	7.4	38.8	9.4	2.6	7.6
SA Temp (℃)	22.4	22.8	28.9	21.7	23.3	22.4
RA Temp (℃)			24.5			
	G (manikin)	H	I	J	K	L
Flow rate (L/s)	9.4	8.7	6.5	8.5	35.2	10.3
SA Temp (℃)	15.7	16.8	17.0	15.8	15.9	16.2
RA Temp (℃)			24.5			

* SA: supply air; RA = return air

Velocity measurements were taken on the symmetric plane of the PV at five heights (0.8, 1.1, 1.2, 1.4, and 1.6 m) along the vertical line at FC (Fig. 5). Figure 6 showed the velocity comparison between the experiment and simulation. Similar results were obtained with the two different boundary conditions, which also agreed reasonably well with the measurements (Fig. 6(a)). The single cubicle case and the whole room case also showed similar trends of jet development (Fig. 6(b)) while the whole room case gives a larger peak value.

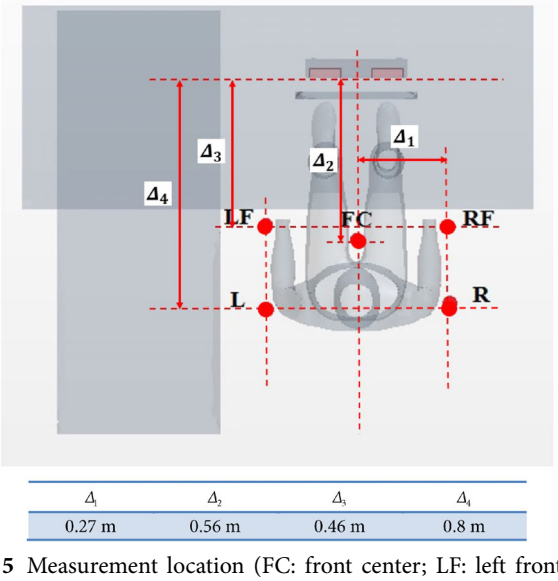

Fig. 5 Measurement location (FC: front center; LF: left front; L: left; RF: right front; R: right)

Temperature measurements were taken along the four vertical poles (RF, R, LF and L) around the manikin at six heights (0.1, 0.6 0.8, 1.1, 1.4, and 1.8 m). The results showed a better agreement obtained by the specified surface temperature compared with the specified surface heat flux (Fig. 7(a)). The whole room case gave almost the same agreement as the single cubicle case did (Fig. 7(b)), which means a simplified single cubicle case is good enough to represent the temperature field.

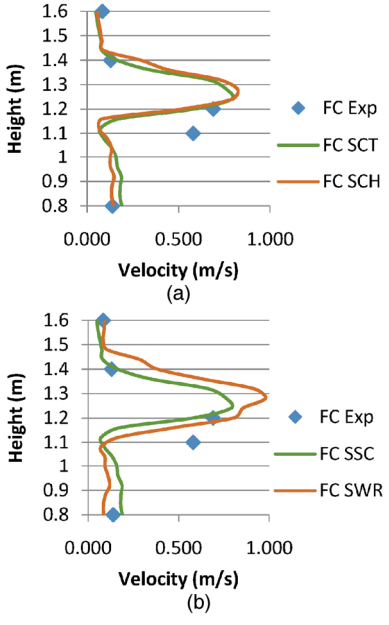

Fig. 6 Velocity validation (a) of different boundary conditions; (b) of different simulation space (Exp: experiment; SCT: simulation of constant temperature; SCH: simulation of constant heat flux; SSC: simulation of single cubicle; SWR: simulation of whole room)

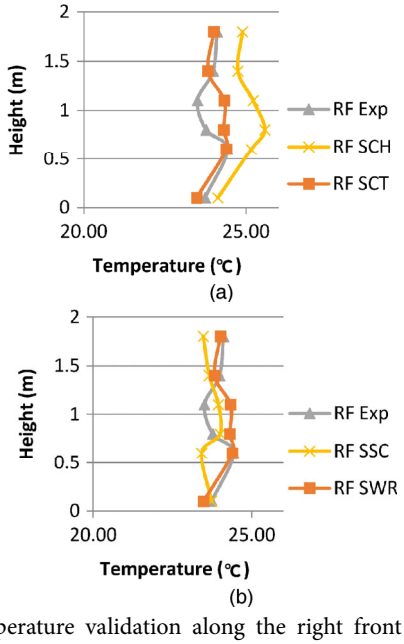

Fig. 7 Temperature validation along the right front pole (a) of different boundary conditions; (b) of different simulation space

3.2 PV and UFAD comparison

Based on the experiment results, an evaluation of thermal comfort based on the equivalent temperature is calculated. Defined by the ISO 14505-2 (2004), "the equivalent temperature is the temperature of a homogeneous space with the mean radiant temperature equal to air temperature and zero air velocity, in which a person exchanges the same heat loss by convection and radiation as in the actual conditions under assessment". After calibration, the heat transfer coefficients for each segment in a homogeneous space have been obtained. Using Eq. (12), the equivalent temperature for each segment can be calculated. The thermal comfort zone given by Nilsson and Holmér (2004) with the calculated equivalent temperature indicates a thermal comfort evaluation for each segment. Overall, PV and UFAD give almost the same thermal comfort level for most segments of the manikin. However the chest, face and scalp in the PV case and the right upper arm in UFAD case are "feeling" colder than the other parts because these parts are exposed to the blowing of supply air. (Fig. 8).

$$t_{eq} = t_s - \frac{q''_t}{h_{teq}} \tag{12}$$

where h_{teq} is the dry heat transfer coefficient, which is determined during calibration in a standard homogeneous environment and t_{eq} is the temperature of the uniform homogeneous environment which is the equivalent temperature (Nilsson and Holmér 2004).

The AQI for evaluating the air quality was calculated with the simulation result. A better performance was achieved by the PV (Fig. 9(a)). In UFAD case, a uniform profile was created in most space of the cubicle due to the strong mixing performance of the UFAD. In contrast, an obvious PV jet

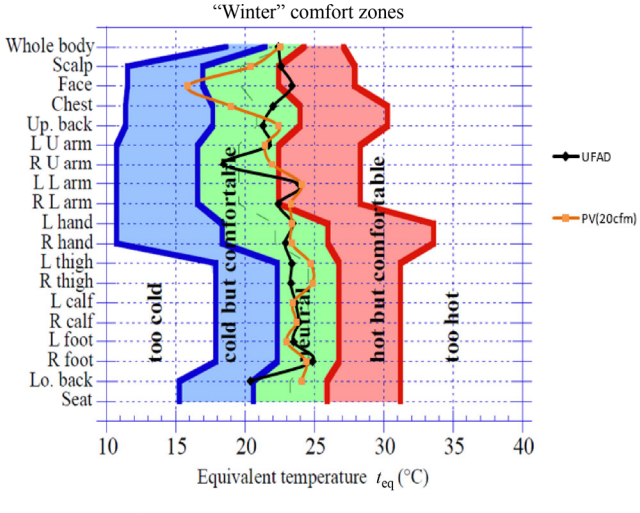

Fig. 8 Equivalent temperature

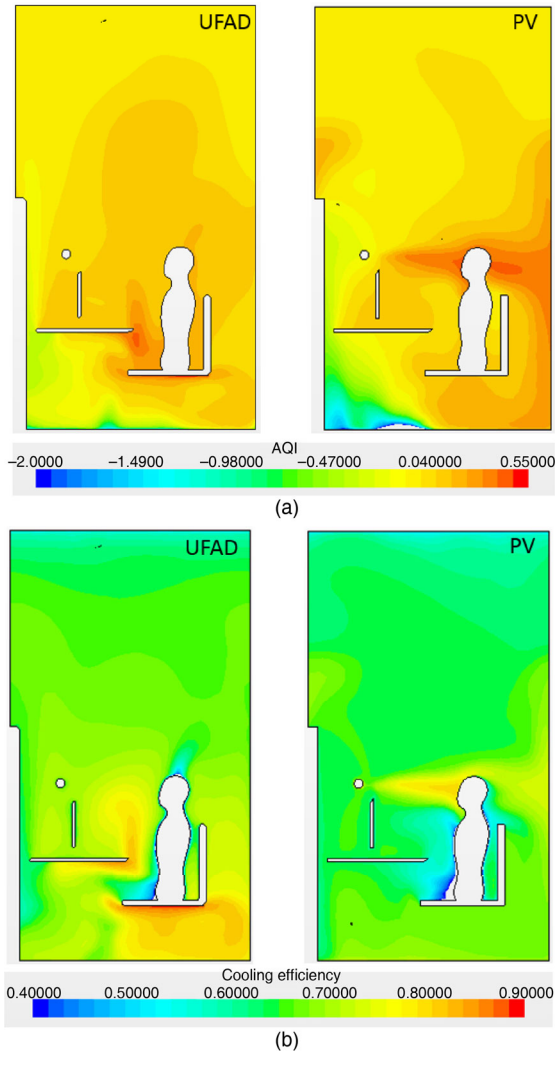

Fig. 9 (a) AQI and (b) cooling efficiency comparison

with cleaner air provided a local dilution in the breathing zone. The AQI in the vicinity of the mouth and nose (breathing zone) given by PV (0.483) was about 4 times of that UFAD provided (0.115). The lowest AQI took place near the floor for both cases but in PV case another low AQI region showed up below the front desk which can be considered as a stagnation region.

As shown in Fig. 9(b), cooling effect acted similarly as the AQI. For the UFAD case, the cooler air was supplied from the floor, some part of the supplied air was firstly obstructed by the chair and front desk, and then spread out and was transported to the region where the manikin was. But for the PV case, cooler air was transported to the manikin's face directly with a little entrainment which led to the lower equivalent temperature at head, face and chest level (Fig. 8), and some part of the cooler air went around the head and then sank down to the floor level due to the heavier density caused by lower temperature.

3.3 PV performance under different airflow rates

In order to investigate the flow field and performance of the PV under different airflow rates. A velocity profile measurement was conducted to give a velocity distribution over the PV outlet. The velocity was measured on a 12 × 5 (× 2) grid (Fig. 10(b)). Based on the measurement, a boundary condition was created in the STAR-CCM (Fig. 10). One can clearly see that the largest velocity took place in the central two slots of the PV especially for the large flow rate (7.1 L/s and 9.4 L/s).

Under different airflow rates, a same specified surface temperature was given for each case. Room temperature increasing (22–25℃) can be seen with decreasing airflow rate in Fig. 11. A jet detouring occurred in the case of 2.4 L/s and 4.7 L/s which was due to a larger density difference and the local cooling region was also changed from head level to stomach. In the case of 7.1 L/s and 9.4 L/s, a remaining jet showed up behind the head of the manikin and spread through the partition of the cubicle, but in the case of 4.7 L/s and 2.4 L/s, the jet was stopped by the manikin and descended to the lower level. The thermal plume at the head level of the manikin was destroyed by the jet of 4.7, 7.1 and 9.4 L/s, but only the one in the 2.4 L/s case still existed.

In the view from the back of the manikin (Fig. 12), our observation was confirmed: a cooler region existed around the manikin head in the cases 7.1 L/s and 9.4 L/s, with a thermal plume going up above the head in the case 2.4 L/s. And the thermal plumes of the cases 7.1 L/s and 9.4 L/s were stopped from the shoulder level but the one of 4.7 L/s was destroyed at lower level.

From the velocity field (Fig. 13), a more obvious flow field was indicated. For the cases of 7.1 L/s and 9.4 L/s, the air supplied by the PV went through the head and spread over the back partition, and most of it dropped to the lower level beneath the chair and was driven back up by the thermal plume. For the cases 4.7 L/s and 2.4 L/s, jet was

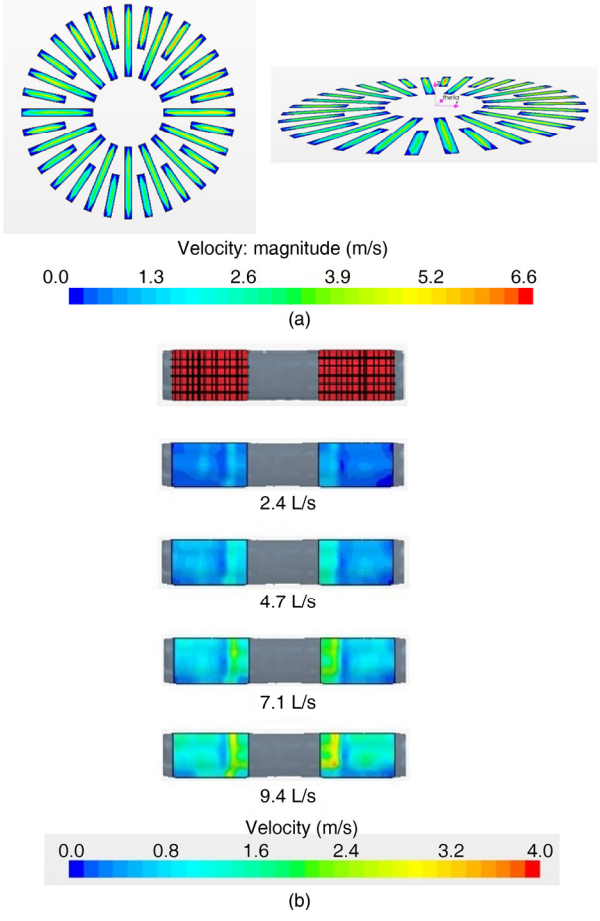

Fig. 10 (a) UFAD and (b) PV outlet velocity profile

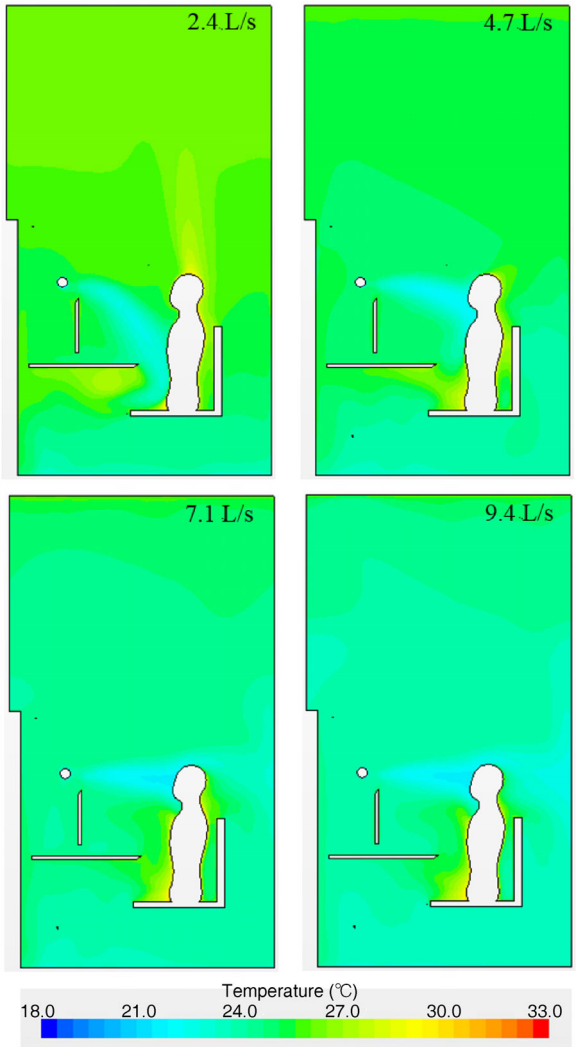

Fig. 11 Temperature distribution at the manikin symmetry plane

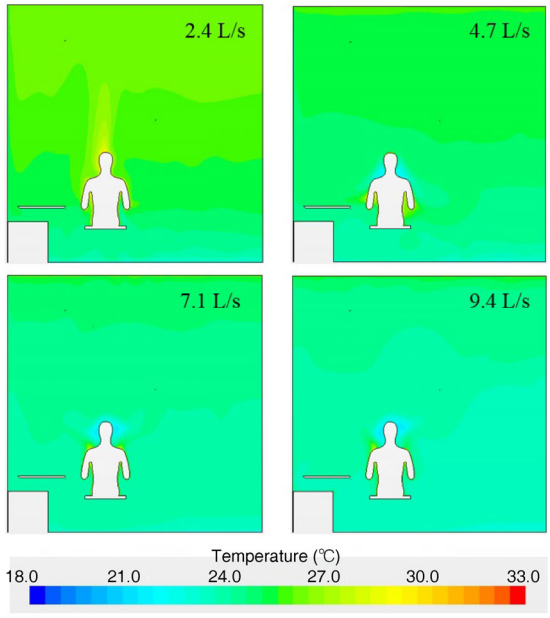

Fig. 12 Back view of the temperature distribution

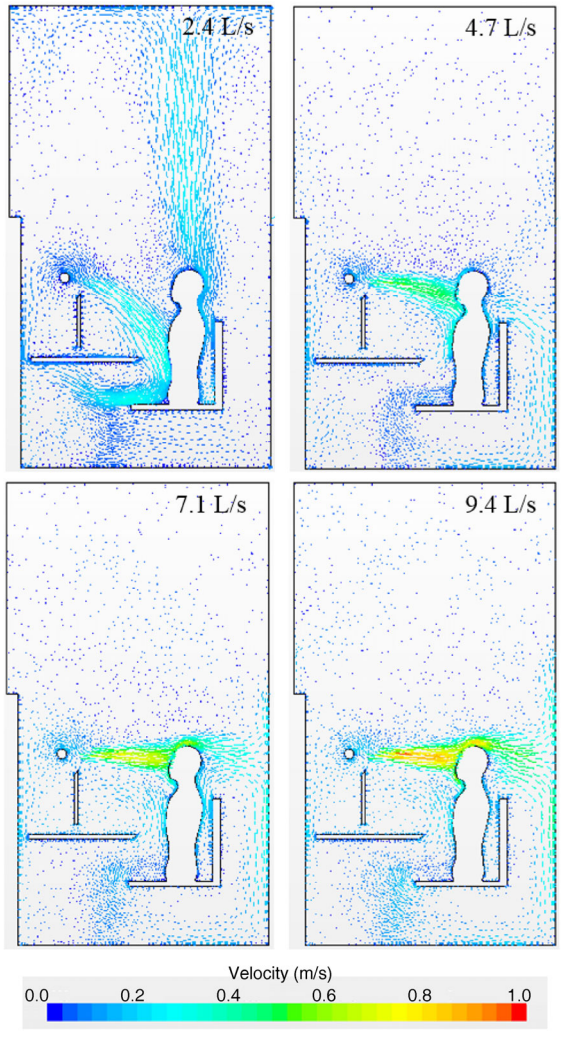

Fig. 13 Velocity field at the manikin symmetry plane

prevented by the manikin and flushed to the lower level through the slot between the manikin and the front desk.

Air quality is also tested with the tracer gas by simulation. SF_6 is emitted from the floor uniformly as the tracer gas at a rate of 1E–6 kg/(m^2·s). After getting to steady state, the mass fraction field at the symmetry plane of the manikin was tested (Fig. 14). One can easily find that, with the airflow rate increasing, the average mass fraction of the contaminant decreased a lot. The highest fraction always took place near the floor. And due to the recirculation flow at the lower part, most of the contaminant was pushed to the front partition. The contaminant fraction at the breathing zone in the 2.4 L/s case (0.29%) was much larger than the other three (0.09%, 0.04% and 0.03% for 4.7, 7.1 and 9.4 L/s) which is resulted from the fact that the jet of 2.4 L/s descended too fast to reach the breathing zone.

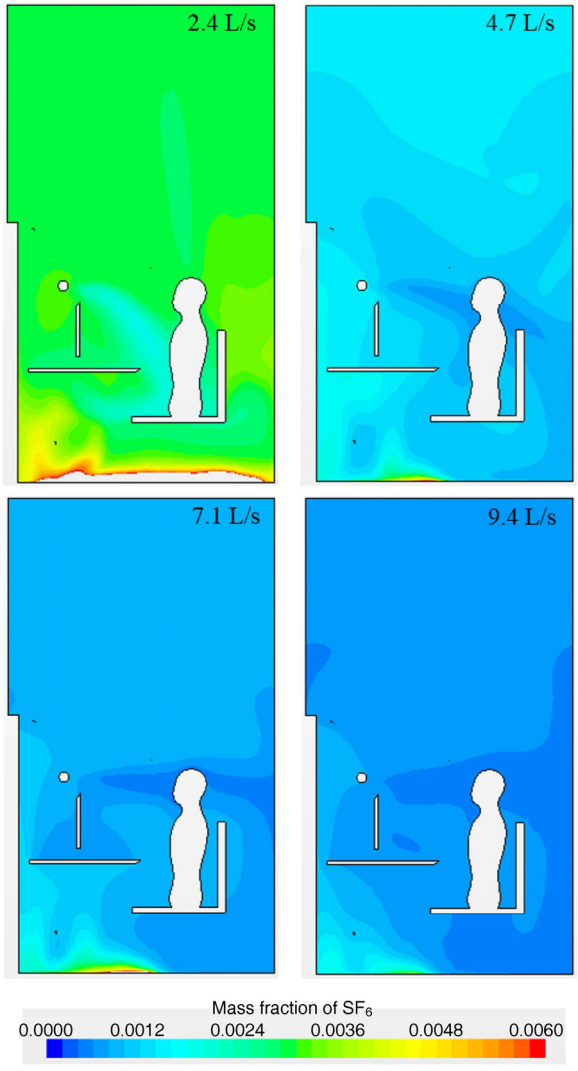

Fig. 14 Tracer gas mass fraction field at the manikin symmetry plane

4 Conclusions

For the investigation of air and air contaminant distributions in a typical cubicle, a computational mesh with a base grid size of 0.05 m was found to have sufficient grid independence. The CFD model with the realizable k–ε turbulence model in combination with the two layer-model were found to provide satisfactory predictions. Compared with the simulation of single office cubicle with periodic boundary conditions, the agreement between predicted and measured results were almost the same in the whole room case. Furthermore, specifying constant surface temperature on the manikin surfaces resulted better predictions than specifying constant heat fluxes.

Comparing UFAD and PV that had about 1/5 air supply flow rate as that of UFAD, PV maintained similar thermal comfort level as the UFAD system except for some body segments. PV system used the supply air more efficiently than UFAD (with AQI 4 times of the UFAD case). Under different airflow rates, PV performed differently. The 7.1 L/s and 9.4 L/s jet acted like isothermal jet, while the 2.4 L/s and 4.7 L/s jet descended to lower levels resulting in cooling region below breathing zone, and higher contaminant fraction in the breathing zone. Overall, personalized ventilation mounted in cubicles could provide a comparatively better thermal and air quality environment around the human body if properly designed and operated.

5 Future work

This paper built a CFD model for simulating the air distribution in a ventilated cubicle. Unlike the previous work done to investigate the performance of personalized ventilation system, this work was aimed at providing a foundation for studying the performance of a partitioned cubicle collaborating with personalized ventilation systems. In the future, the partitioned cubicle with different design factors, such as some configuration parameters, will be studied to enrich the knowledge of the ventilated partitioned cubicles and help to develop a method for designing it.

Acknowledgements

We gratefully acknowledge the support of Syracuse Center of Excellence Building for the use of TIEQ lab, and that of Dr. Dang for the access to the STAR CCM software.

References

Cermak R, Melikov AK, Foreijt L, Kovar O (2011). Performance of personalized ventilation in conjunction with mixing and displacement ventilation. *HVAC&R Research*, 12: 295–311.

Chen Q, Xu W (1998). A zero-equation turbulence model for indoor air flow simulation. *Energy and Building*, 28: 137–144.

Chludzinska M, Bogdan A (2008). Individual ventilation—Users' whim or economically justified energy saving. *Ciepłownictwo, Ogrzewnictwo, Wentylacja*, 2: 32–34 (in Polish).

Dang T (2008). Personalized ventilation system using combined jet nozzle and flow suction. US Provisional Patent No. 61/022956.

Deevy M, Sinai Y, Everitt P, Voigt L, Gobeau N (2008). Modelling the effect of an occupant on displacement ventilation with computional fluid dynamics. *Energy and Buildings*, 40: 255–264.

Dygert RK, Dang TQ (2012). Experimental validation of local exhaust strategies for improved IAQ in aircradt cabins. *Building and Environment*, 47: 76–88.

Dygert RK, Russo JS (2009). Modeling of the human body to study the personal micro environment. *ASHRAE Transactions*, 115(2): 407–420.

Gao N, Niu J (2004). CFD study on mocro-environment around human body and personalized ventilation. *Building and Environment*, 39: 795–805.

Gao N, Niu J (2005). Modeling the performance of personalized ventilation under different room airflows. In: Proceedings of IBPSA International Conference, Montreal, Canada.

Gao N, Niu J (2006). Transient CFD simulation of the respiration process and interperson exposure assessment. *Building and Environment*, 41: 1214–1222.

Hayashi T, Ishizu Y, Kato S, Murakami S (2002). CFD analysis on characteristics of contaminated indoor air ventilation and its application in the evaluation of the effects of contaminant inhalation by a human occupant. *Building and Environment*, 37: 219–230.

Houdas Y, Ring E (1982). Human Body Temperature: Its Measurement and Regulation. New York: Plenum Press.

ISO 14505-2. (2006). Ergonomics of the thermal environment—Evaluation of the thermal environments in vehicles—Part 2: Determination of equivalent temperature. ISO Standard.

Kaczmarczyk J, Melikov AK, Fanger PO (2004). Human response to personalized ventilation and mixing ventilation. *Indoor Air*, 14(suppl 8): 17–29.

Khalifa EH, Janos MI, Dannenhoffer JF (2009). Experimental investigation of reduced-mixing personal ventilation jets. *Building and Environment*, 44: 1551–1558.

Khalifa EH, Prescod SJ, Dannenhoffer JF, Elhadidi B (2006). Computation of occupant exposure in an office cubicle. In: Proceedings of AWMA/EPA Conference: Indoor Air Quality—Problems, Research and Solutions, Durham, USA.

Melikov AK (2004). Improving comfort and health by personalized ventilation. In: Proceedings of Roomvent 2004, Coimbra, Portugal.

Melikov AK, Cermak R, Majer M (2002). Personalized ventilation: Evaluation of different air terminal devices. *Energy and Building*, 34: 829–836.

Melikov AK, Dzhartov V (2013). Advanced air distribution for minimizing airborne cross-infection in aircradt cabin. *HVAC&R Research*, 19: 926–933.

Nielsen PV, Barszcz E, Czarnota T, Dymalski DP, Jasienski MA, Nowotka A, Nowotka A, Mozer A, Wiankowska SM, Jensen RL (2008). The influence of draught on a seat with integrated personalized ventilation. In: Proceedings of Indoor Air 2008, 11th International Conference in Indoor Air Quality and Climate, Copenhagen, Denmark.

Nielsen PV, Bartholomaeussen NM, Jakubowska E, Jiang H, Jonsson OT, Krawiecka K, Mierzejewski A, Jessica SJ, Trampczynska K, Polak M, Soennichsen M (2007a). Chair with integrated personalized ventilation for minimizing cross infection. In: Proceedings of Roomvent 2007, 10th International Conference on Air Distribution in Rooms, Helsinki, Finland.

Nielsen PV, Damsgaard C, Liu L, Jensen RL (2013). Test of different air distribution concepts for a single-aisle aircraft cabin. In: Proceedings of CLIMA 2013, Prague, Czech Republic.

Nielsen PV, Hyldgard CE, Melikov A, Andersen H, Soennichsen M (2007b). Personal exposure between people in a room ventilated by texile terminals: with and without personalized ventilation. *HVAC&R Research*, 13: 635–644.

Nielsen PV, Jiang H, Polak M (2007c). Bed with integrated personalized ventilation for minimizing cross infection. In: Proceedings of Roomvent 2007, 10th International Conference on Air Distribution in Rooms, Helsinki, Finland.

Nilsson HO, Holmér I (2004). Comfort climate evaluation with thermal manikin methods and computer simulation models, *Indoor Air*, 13: 28–37.

Russo JS (2010). A detailed and Systematic Investigation of Personal Ventilation Systems. Phd Dissertation, Syracuse University.

Russo JS, Dang TQ, Khalifa EH (2009). Computational analysis of reduced-mixing personal ventilation jets. *Building and Environment,* 44: 1559–1567.

STAR-CCM. (2012). Tutorial Guide of STAR-CCM .

Vander JA, Sherman HJ, Luciano SD (1994). Human Physiology: The Mechanisms of Body Function. New York: McGraw-Hill.

Villi G, Carli MC (2014). Detailing the effects of geometry approximation and grid simplification on the capability of a CFD model to address the benchmark test case for flow around a computer simulated person. *Building Simulation,* 7: 35–55.

Xu W, Chen Q (2000). Simulation of mixed convection flow in a room with a two-layer turbulence model. *Indoor Air*, 10: 306–314.

Xu W, Chen Q (2001). A two-layer turbulence model for simulating indoor airflow Part II. Applications. *Building and Environment,* 33*:* 627–639.

Zhuang R, Li X, Tu J (2014). CFD study of the effects of furniture layout on indoor air quality under typical office ventilation schemes. *Building Simulation,* 7: 263–275.